Real-Time Imaging of Cellulose Reorientation during Cell Wall Expansion in Arabidopsis Roots[1][W][OA]

Charles T. Anderson[2], Andrew Carroll[2], Laila Akhmetova, and Chris Somerville*

Energy Biosciences Institute (C.T.A., A.C., L.A., C.S.) and Department of Plant and Microbial Biology (C.S.), University of California, Berkeley, California 94720; and Department of Biology, Stanford University, Stanford, California 94305 (A.C.)

Cellulose forms the major load-bearing network of the plant cell wall, which simultaneously protects the cell and directs its growth. Although the process of cellulose synthesis has been observed, little is known about the behavior of cellulose in the wall after synthesis. Using Pontamine Fast Scarlet 4B, a dye that fluoresces preferentially in the presence of cellulose and has excitation and emission wavelengths suitable for confocal microscopy, we imaged the architecture and dynamics of cellulose in the cell walls of expanding root cells. We found that cellulose exists in Arabidopsis (*Arabidopsis thaliana*) cell walls in large fibrillar bundles that vary in orientation. During anisotropic wall expansion in wild-type plants, we observed that these cellulose bundles rotate in a transverse to longitudinal direction. We also found that cellulose organization is significantly altered in mutants lacking either a cellulose synthase subunit or two xyloglucan xylosyltransferase isoforms. Our results support a model in which cellulose is deposited transversely to accommodate longitudinal cell expansion and reoriented during expansion to generate a cell wall that is fortified against strain from any direction.

The walls of growing plant cells must fulfill two simultaneous and seemingly contradictory requirements. First, they must expand to accommodate cell growth, which is anisotropic in many tissues and determines organ morphology. Second, they must maintain their structural integrity, both to constrain the turgor pressure that drives cell growth and to provide structural rigidity to the plant. These requirements are met by constructing primary cell walls that can expand along with growing cells, whereas secondary cell walls are deposited after cell growth has ceased and serve the latter function.

One of the major constituents of both types of cell walls is cellulose, which exists as microfibrils composed of parallel β-1,4-linked glucan chains that are held together laterally by hydrogen bonds (Somerville, 2006). Microfibrils are 2 to 5 nm in diameter, can extend to several micrometers in length, and exhibit high tensile strength that allows cell walls to withstand turgor pressures of up to 1 MPa (Franks, 2003). In vascular plants, cellulose is synthesized by a multimeric cellulose synthase (CESA) complex composed of at least three types of glycosyl transferases arranged into a hexameric rosette (Somerville, 2006). After delivery to the plasma membrane, CESA initially moves in alignment with cortical microtubules (Paredez et al., 2006), but its trajectory can be maintained independently of microtubule orientation. For example, in older epidermal cells of the root elongation zone in Arabidopsis (*Arabidopsis thaliana*), cellulose microfibrils at the inner wall face are oriented transversely despite the fact that microtubules reorient from transverse to longitudinal along the elongation zone (Sugimoto et al., 2000), suggesting that microtubule orientation and cellulose deposition are independent in at least some cases.

Depending on species, cell type, and developmental stage, cellulose microfibrils may be surrounded by additional networks of polymers, including hemicelluloses, pectins, lignin, and arabinogalactan proteins (Somerville et al., 2004). Hemicelluloses are composed of β-1,4-linked carbohydrate backbones with side branches and include xyloglucans, mannans, and arabinoxylans. Xyloglucan is thought to interact with the surface of cellulose and form cross-links between adjacent microfibrils (Vissenberg et al., 2005). In some cell types, pectin or lignin may also participate in cross-linking or entrapment of other cell wall polymers. It is unclear how the associations between networks of different cell wall components are relaxed to allow for cell wall expansion during growth.

Several models have been proposed for the behavior of cell wall components during wall expansion. The passive reorientation hypothesis (also called the multinet growth hypothesis; Preston, 1982) postulates that in longitudinally expanding cells, cellulose microfibrils are synthesized in a transverse pattern and are then reoriented toward the longitudinal axis due to the

[1] This work was supported by the Energy Biosciences Institute and by the U.S. Department of Energy (grant no. DE–FG02–09ER16008).

[2] These authors contributed equally to the article.

* Corresponding author; e-mail crs@berkeley.edu.

The author responsible for distribution of materials integral to the findings presented in this article in accordance with the policy described in the Instructions for Authors (www.plantphysiol.org) is: Chris Somerville (crs@berkeley.edu).

[W] The online version of this article contains Web-only data.

[OA] Open Access articles can be viewed online without a subscription.

www.plantphysiol.org/cgi/doi/10.1104/pp.109.150128

strain generated by turgor pressure (Green, 1960). This phenomenon has been observed in the multicellular alga *Nitella* (Taiz, 1984). In higher plants, there is less direct evidence for passive reorientation, and another hypothesis holds that wall expansion involves active, local, and controlled remodeling of cellulose microfibrils along a diversity of orientations (Baskin, 2005). Such remodeling could be achieved by proteins such as xyloglucan endotransglycosylases (XETs), which break and rejoin xyloglucan chains, and expansins, which loosen cell walls in vitro in a pH-dependent manner (Cosgrove, 2005). Marga et al. measured cellulose microfibril orientation at the innermost layer of the cell wall before and after in vitro extension and did not observe reorientation (Marga et al., 2005). This suggests that processes other than microfibril reorientation might be involved in wall expansion, at least under certain circumstances or in some wall layers. Thus, the degree to which cellulose microfibrils are reoriented after their synthesis during wall expansion has remained unclear.

One difficulty in resolving this problem has been the inability to directly image cellulose microfibrils in the growing cell wall. Existing methods to assess cellulose structure and orientation in plant cell walls are limited by the low contrast of cellulose in transmission electron microscopy, the ability to image only the surface of the wall using field emission scanning electron microscopy, and the use of polarized light microscopy in combination with dyes such as Congo red to measure only the bulk orientation of cellulose microfibrils (Baskin et al., 1999; Sugimoto et al., 2000; Verbelen and Kerstens, 2000; MacKinnon et al., 2006). In addition, the sample manipulation required for the former two methods has the potential to introduce artifacts (Marga et al., 2005). Although cellulose microfibril orientation differs at the inner and outer surfaces of the cell wall (Sugimoto et al., 2000) and presumably changes over time, the dynamics of cellulose reorientation during cell wall expansion have not been observed to date.

In this study, we tested fluorescent dyes for their potential to allow imaging of cellulose distribution in the walls of Arabidopsis seedlings by confocal microscopy. We used one of these dyes to characterize the distribution of cellulose in wild-type root cells and in mutants with reduced cellulose or xyloglucan. By directly observing the fine structure of cellulose over time in growing wild-type root cells, we concluded that cellulose microfibrils in these cells reorient in a transverse to longitudinal direction as predicted by the passive reorientation hypothesis.

RESULTS

Characterization of Fluorescent Carbohydrate-Binding Dyes

To enable imaging of cellulose structure in intact plant cell walls, we characterized fluorescent dyes previously described as cell wall stains for fungi, Solophenyl Flavine 7GFE (7GFE) and Pontamine Fast Scarlet 4B (S4B; Hoch et al., 2005), and Calcofluor, which has been widely used to stain cell wall components (Sauter et al., 1993; Fig. 1A; Supplemental Fig. S1). We used fluorimetry to measure dye fluorescence in the presence of isolated cell wall carbohydrates and polysaccharide standards. Interaction with certain carbohydrates led to greatly increased dye fluorescence (Table I). All three dyes showed increased fluorescence in the presence of xyloglucan or cellulose, and the fluorescence of 7GFE and S4B with cellulose was greatly enhanced in 50 to 150 mM NaCl or KCl solutions. The latter phenomenon might be due to a requirement for cation binding for dye-carbohydrate interaction. All three dyes also displayed a lesser increase in fluorescence in the presence of curdlan, a chain of β-1,3-linked glucans that is similar to callose (Stone et al., 1984). 7GFE also displayed increased fluorescence in solutions of lichenan and glucomannan. Of the three dyes, Calcofluor was the most promiscuous, whereas 7GFE and S4B were more selective for polysaccharides containing β-1,4 linkages (Table I). The dye structures (Fig. 1A; Supplemental Fig. S1) are reminiscent of the surfaces of carbohydrate binding modules, which are thought to interact with their substrates via sets of aromatic amino acid side chains (Boraston et al., 2004).

In the presence of xyloglucan, the emission maximum of 7GFE visibly shifted to a shorter wavelength, whereas this shift did not occur in the presence of cellulose (Supplemental Fig. S2). We recorded the emission spectra of 7GFE in phosphate-buffered saline (PBS) alone and in PBS containing xyloglucan or cellulose after excitation over a range of wavelengths (Supplemental Figs. S1 and S2). 7GFE fluorescence was more intense with xyloglucan than with cellulose upon excitation at wavelengths between 460 and 470 nm, whereas fluorescence was more intense with cellulose upon excitation at 442 nm (Supplemental Fig. S1). Similar analysis of S4B indicated that fluorescence was much more intense in the presence of cellulose than xyloglucan at all excitation wavelengths (Fig. 1B). Under all conditions, 7GFE and S4B exhibited strong fluorescence when excited with light between 230 and 400 nm, whereas mixing with polysaccharides caused the formation of an additional fluorescence peak in the visible spectrum that approached or exceeded the intensity of their UV-range fluorescence (Fig. 1, C and D; Supplemental Fig. S2). Because S4B fluoresced much more brightly in the presence of cellulose than with any other polysaccharide tested (Table I), we chose this dye to investigate the spatial distribution of cellulose in plant cell walls.

S4B Staining Reveals the Three-Dimensional Architecture of Cellulose in Root Cells

S4B was used to label the cell walls of 5-d-old light-grown Arabidopsis seedlings of the Columbia (Col)

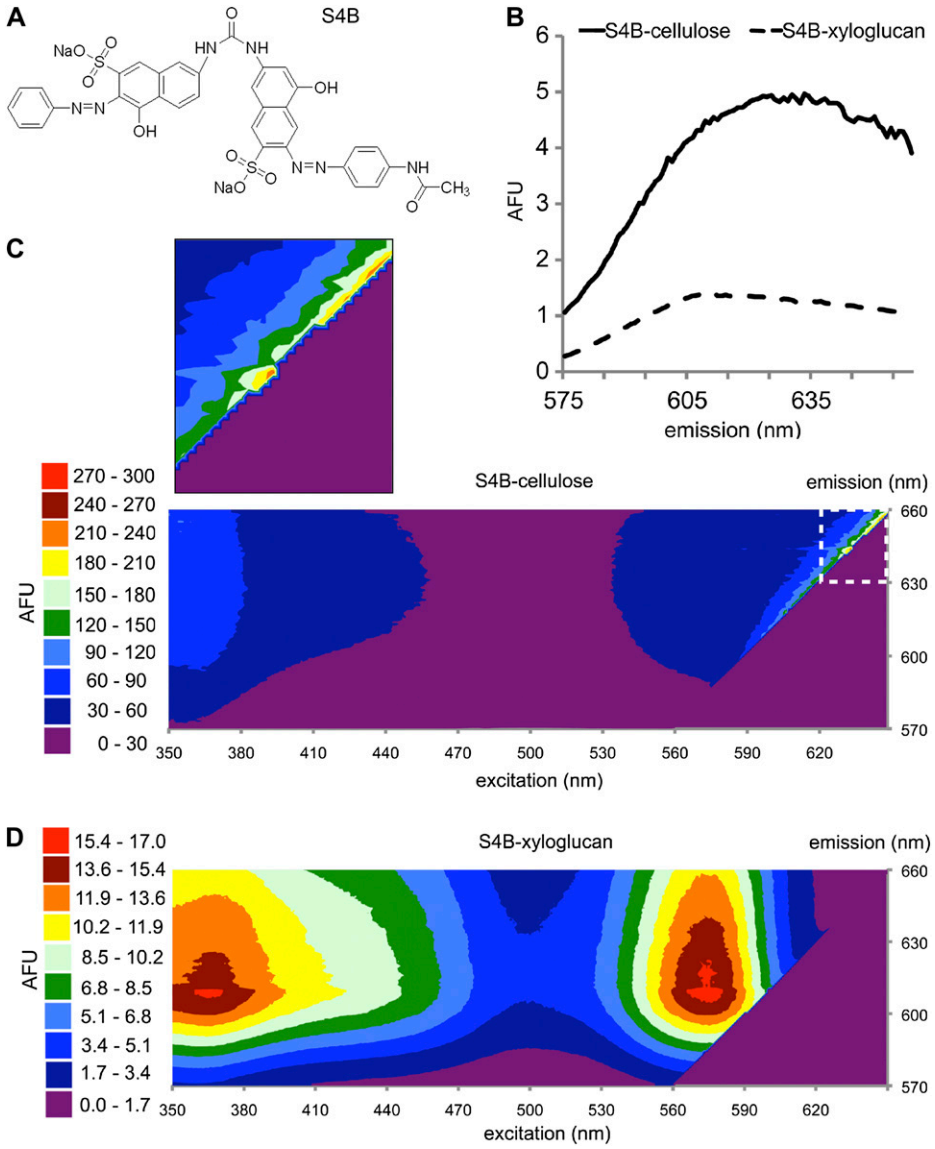

Figure 1. S4B becomes highly fluorescent upon cellulose binding. A, Structure of S4B. B, Profiles of emission intensities for S4B after excitation at 561 nm in solutions containing equal masses of xyloglucan (dotted line) or cellulose (solid line). AFU, Arbitrary fluorescence units. C, Contour plot of fluorescence recorded across a range of excitation and emission wavelengths for S4B in a cellulose mixture. Enlarged area (dashed box) shows sharp fluorescence peak in visible wavelengths. D, Similar contour plot for S4B in a xyloglucan solution. Note the difference in scales for plots in C and D.

ecotype. The aerial organs of Arabidopsis are covered in a waxy cuticle that inhibited dye entry, but roots readily took up the dye. In addition, cells at the root apex divide, elongate, and differentiate in a defined pattern (Dolan et al., 1993) that allows for the simultaneous imaging of cell walls at different developmental stages. Maximum intensity projections of z series collected by spinning disc confocal microscopy of stained seedlings revealed fibrillar staining patterns that were absent in unstained controls and varied along the length of the root (Fig. 2A). In the columella and lateral root cap cells near the root tip, finely spaced transverse fibrillar staining was evident (Fig. 2B). This pattern gave way to thicker, widely spaced diagonal fibrillar structures in older lateral root cap cells (Fig. 2C). Epidermal cells in the elongation and differentiation zones displayed a crosshatched pattern of finely spaced fibrillar staining (Fig. 2, D and E). We analyzed the orientation of the fibrillar staining in successive z slices and observed longitudinal fibrillar staining at the outer surface of the cell wall that transitioned to a transverse/diagonal pattern at the inner surface of the wall (Fig. 3A). Leftward- and rightward-tilted diagonal fibers coexisted in single cells (Fig. 2C), indicating that the handedness of cellulose fiber tilting was not restricted to one direction.

These fibrillar staining patterns were reminiscent of wide-field images of Calcofluor staining in cotton (*Gossypium hirsutum*) fibers (Sauter et al., 1993) and of XET activity in root cells that likely reflects cellulose-associated xyloglucans (Vissenberg et al., 2005). In agreement with the latter result, we observed a fibrillar pattern reminiscent of S4B staining in root cells incubated with 0.01% aqueous Congo red (data not shown), even though Congo red interacts preferentially with xyloglucan over cellulose (Wood, 1980). We

Table I. *Relative fluorescence of dyes in the presence of carbohydrates*

The fluorescence intensity of S4B and 7GFE increases in the presence of specific carbohydrates. Fluorescence of S4B, 7GFE, or Calcofluor incubated with carbohydrates (see "Materials and Methods" for sources) relative to their fluorescence in control solutions (water or PBS). X = excitation wavelength, M = emission wavelength. Each dye's relative fluorescence values are standardized to its own control value. Errors are SD from 12 wells for each mixture.

Carbohydrate	S4B	7GFE	Calcofluor	Calcofluor
	X = 535 nm, M = 595 nm	*X = 485 nm, M = 535 nm*	*X = 360 nm, M = 465 nm*	*X = 485 nm, M = 535 nm*
PBS control	1.00 ± 0.0448	1.00 ± 0.019	–	–
Water control	–	–	1.00 ± 0.0582	1.00 ± 0.281
Cellulose	64.4 ± 0.956	39.0 ± 7.11	2.53 ± 0.228	19.3 ± 2.84
Xyloglucan	14.6 ± 2.93	12.8 ± 4.35	3.75 ± 0.228	1.47 ± 0.428
Curdlan	3.28 ± 0.200	3.03 ± 0.896	1.88 ± 0.622	0.965 ± 0.230
Glucomannan	1.02 ± 0.528	8.17 ± 0.548	0.962 ± 0.548	1.47 ± 0.0618
Lichenan	1.26 ± 0.504	8.93 ± 1.16	3.50 ± 0.619	15.2 ± 2.51
Arabinan	1.20 ± 0.0845	0.776 ± 0.114	0.751 ± 0.0367	9.01 ± 0.473
Arabinogalactan	1.13 ± 0.102	1.05 ± 0.0899	0.909 ± 0.0524	1.86 ± 0.0875
Arabinoxylan	0.951 ± 0.0802	0.918 ± 0.106	0.841 ± 0.0278	3.19 ± 1.50
Cellobiose	0.856 ± 0.100	0.870 ± 0.0937	0.917 ± 0.0763	0.901 ± 0.113
Cellotriose	0.963 ± 0.0910	0.836 ± 0.107	1.12 ± 0.105	1.04 ± 0.0965
Cellotetrose	0.834 ± 0.0842	0.889 ± 0.113	0.973 ± 0.0639	0.882 ± 0.152
Cellopentose	1.15 ± 0.0983	1.17 ± 0.0905	0.812 ± 0.101	0.888 ± 0.0929
Cellohexose	0.940 ± 0.104	0.914 ± 0.105	1.12 ± 0.158	0.915 ± 0.113
Galactomannan	0.714 ± 0.109	1.20 ± 0.101	0.762 ± 0.0664	27.9 ± 1.59
Isoprimeverose	1.27 ± 0.107	0.835 ± 0.0938	1.03 ± 0.0574	1.34 ± 0.297
Mannan	1.23 ± 0.0975	1.10 ± 0.0884	0.947 ± 0.0452	4.09 ± 0.259
Pectic galactan	0.821 ± 0.0930	1.04 ± 0.117	0.962 ± 0.0449	117.6 ± 3.74
Rhamnogalacturonan	1.17 ± 0.0884	1.01 ± 0.0998	0.873 ± 0.0966	0.873 ± 0.0966
Starch	0.837 ± 0.0932	0.941 ± 0.0838	0.911 ± 0.0655	1.82 ± 0.211
Xylan	1.08 ± 0.0810	1.05 ± 0.103	1.47 ± 0.0545	10.5 ± 0.506

also noticed bright, amorphous S4B staining at root hair primordia in trichoblasts (Fig. 2E), which possibly reflects changes in cell wall structure at these locations. This bright staining could reflect an increase in the amount or accessibility of cellulose at these locations, but could also reflect an accumulation of some other wall component that fluoresces more weakly with S4B such as xyloglucan or callose.

Imaging and Measurement of Cellulose Dynamics during Wall Expansion

The above data and previous results (Sugimoto et al., 2000) indicate that the arrangement and orientation of cellulose microfibrils differ between the inner and outer wall faces in root cells. Because cellulose is synthesized transversely at the inner wall face throughout the elongation zone in roots of Arabidopsis (Sugimoto et al., 2000) and maize (*Zea mays*; Baskin et al., 1999), we hypothesized that cellulose microfibrils synthesized early in the elongation process are reoriented as subsequent cell wall layers with larger initial surface areas are synthesized beneath them. To directly test this idea, we performed time-lapse microscopy of lateral root cap and root epidermal cells that had been stained for 30 min with S4B. In lateral root cap cells, the thick fibrillar structures rotated toward the longitudinal axis in expanding cells, and in elongating epidermal cells, fine fibrillar structures rotated similarly (Fig. 3B; Supplemental Movie S1). We measured the change in fiber angle relative to the long axis of the cell for 22 fibers in epidermal cells from four experiments and found that the fibers rotated in a transverse to longitudinal direction at an average rate of 0.16 ± 0.11 (SD) degrees/min. This rate would result in the rotation of cellulose microfibrils from transverse to longitudinal in 9 h and 22 min, which is similar to calculated residence times for epidermal cells in the root elongation zone (Beemster and Baskin, 1998). The rate of fibrillar rotation varied considerably within single cells, possibly reflecting different physical characteristics between different cell wall regions, and between cells at different positions along the root, possibly reflecting their differing rates of elongation (Sugimoto et al., 2000). We calculated the strain rates of these fibers using the formula: strain rate (%/h) = $(1/\cos\theta_i)^*(\cos\theta_f - \cos\theta_i)/(dt)$, where θ_i is the initial angle relative to the longitudinal cell wall, θ_f is the final angle relative to the longitudinal cell wall, and dt is the elapsed time in hours, and found that the average strain rate was 30.8%/h. In many cases we observed an apparent decrease in the tangential diameter of the cell during the time-lapse recordings (e.g. Supplemental Movie S1). In *procuste1-1* (*prc1-1*) seedlings, cellulose fiber rotation was not as evident as for Col seedlings (Supplemental Movie S2) and could not be reliably measured, suggesting that normal cellulose architecture might be required for fiber rotation to observably occur.

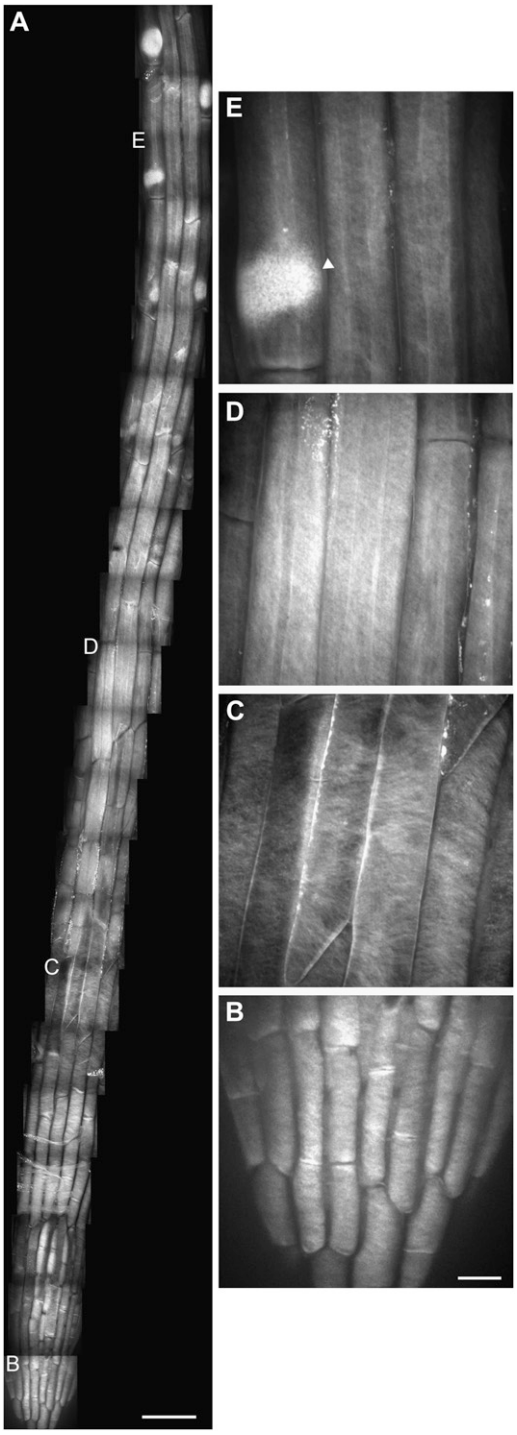

Figure 2. S4B staining pattern in Arabidopsis root cells. A, Mosaic of micrographs of the division, elongation, and early differentiation zones in a 5-d-old light-grown Col seedling stained with S4B. Smaller letters correspond to enlargements in B to E. B, Enlargement of root tip showing finely spaced fibrillar staining. C, Enlargement of lateral root cap showing widely spaced diagonal fibrillar staining. D, Enlargement of elongation zone showing finely spaced longitudinal and diagonal fibrillar staining. E, Enlargement of differentiation zone showing bright staining of root hair primordium in trichoblast (arrowhead). All images are maximum projections of z series. Scale bars are 50 μm (A) or 10 μm (for B–E).

S4B Staining Reveals Altered Patterns of Cellulose Architecture in Cell Wall Mutants

We sought to characterize the spatial distribution of cellulose in cell wall mutants. Roots of *prc1-1* seedlings, which lack the CESA6 subunit of the CESA complex (Desnos et al., 1996) and have reduced cellulose content (MacKinnon et al., 2006), were stained with S4B and observed using confocal microscopy (Fig. 4). Although the fibrillar S4B staining pattern in cells at the root tip of *prc1-1* seedlings was qualitatively similar to that of wild-type seedlings (Fig. 4B), large gaps were present in the fibrillar staining pattern in lateral root cap

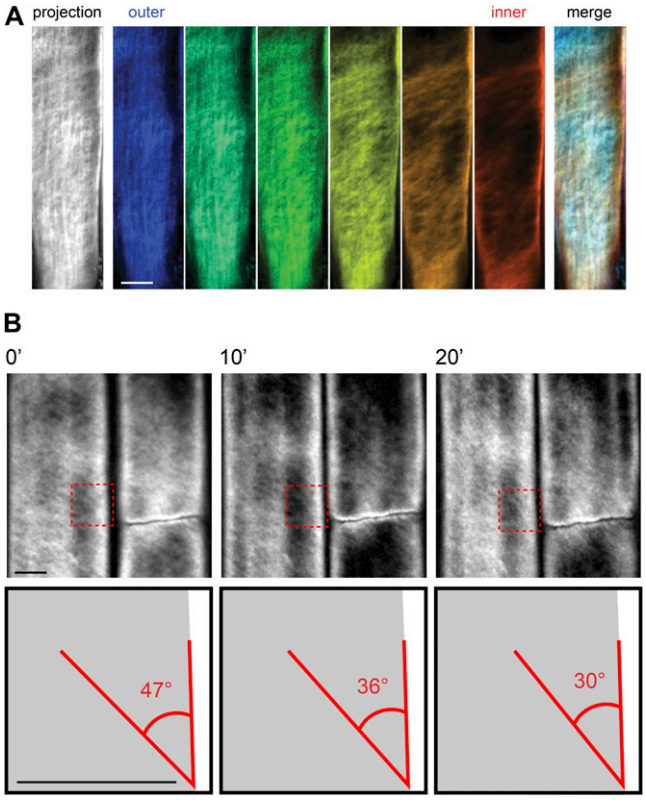

Figure 3. S4B staining allows imaging of cellulose architecture and dynamics. A, Imaging of cellulose orientation in different cell wall layers using S4B staining. Left section, maximum projection of z series through the cell wall in a 7-d-old light-grown Col seedling stained with S4B. Middle sections, pseudocolor-coded slices from the same z series progressing from the outer surface (blue) to the inner surface (red) of the cell wall, with the fibrillar staining pattern transitioning from longitudinal to transverse/diagonal. Spacing between z slices is 200 nm. Right section, merge of pseudocolor-coded slices showing different orientations of fibrillar staining in the outer and inner wall layers. B, Rotation over time of fibrillar staining in elongation zone epidermal cells stained with S4B. Top sections, time points (0′, 10′, 20′) from a time-lapse recording (see Supplemental Movie S1) of an elongating root epidermal cell in a 5-d-old light-grown Col seedling stained with S4B. Bottom sections, cartoon representation of boxes in top sections. The angle between a fibrillar structure and the long axis of the cell decreases from 47° to 30° over 20′. Note that a cell with extraordinarily rapid fiber rotation was chosen for illustrative purposes. Scale bars are 5 μm.

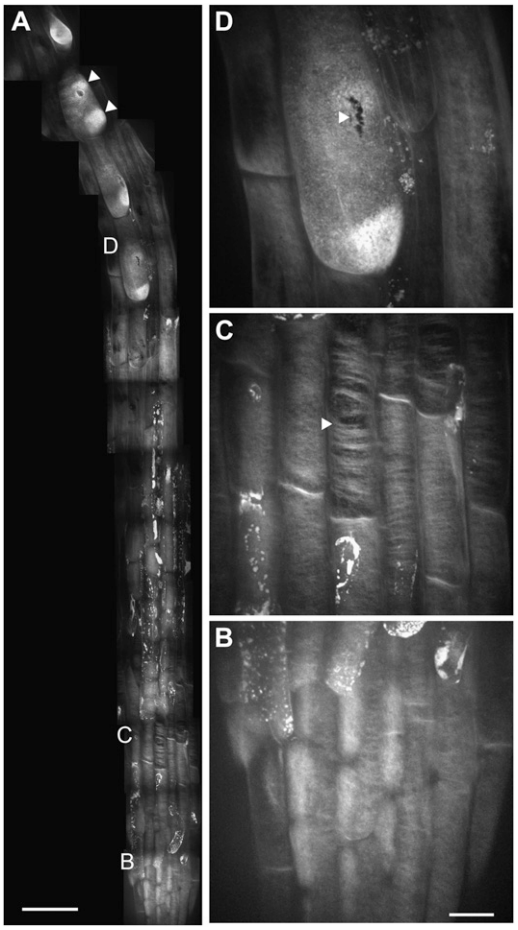

Figure 4. S4B staining pattern in *prc1-1* root cells. A, Mosaic of micrographs from a 5-d-old light-grown *prc1-1* seedling stained with S4B. Arrowheads show multiple bright patches in a single trichoblast. Irregular bright staining along root likely represents dead cells that have absorbed S4B. B, Enlargement of root tip cells showing fibrillar staining. C, Enlargement of lateral root cap cells showing large gaps in thick, curved fibrillar staining (e.g. arrowhead). D, Enlargement of differentiation zone cell showing rupture in trichoblast cell wall (arrowhead). All images are maximum projections of z series. Scale bars are 50 μm (A) or 10 μm (for B–D).

cells (Fig. 4C). This result suggests that although some cellulose is produced in *prc1-1* seedlings, it is distributed less continuously than in wild-type cells (MacKinnon et al., 2006). Some *prc1-1* trichoblasts contained multiple bright patches of S4B staining (Fig. 4A), possibly reflecting precursors for the growth of multiple root hairs from single cells, which occurs in this mutant (Singh et al., 2008). We also noticed small ruptures in the walls of some trichoblasts (Fig. 4D), which we interpret as reflecting the weakened integrity of *prc1-1* cell walls (Desnos et al., 1996). In time-lapse recordings of *prc1-1* seedlings, we occasionally observed ruptures forming in the walls of some cells (Supplemental Movies S3 and S4), providing further evidence for cell wall weakening in this mutant.

We next investigated the distribution of cellulose in *xxt1;xxt2* double-mutant seedlings, which lack detectable xyloglucan in their cell walls (Cavalier et al., 2008). There was a marked decrease in the intensity of S4B fluorescence in *xxt1;xxt2* seedlings as compared to wild type. Although the tissue-wide pattern of S4B staining was similar to that of wild-type seedlings, S4B-stained fibers in elongating cells of *xxt1;xxt2* seedlings (Fig. 5B) were more widely spaced than in wild type (Fig. 5, A and C). In addition, root hair primordia did not stain brightly with S4B in *xxt1;xxt2* mutants (Fig. 5D), possibly reflecting reduced levels of cellulose at these locations relative to wild type. This mutant displays root hair defects (Cavalier et al., 2008), and the lack of S4B staining might reflect an abnormality in the root hair primordium that underlies these defects. As for *prc1-1* seedlings, we observed ruptures in the cell wall of some trichoblasts in *xxt1;xxt2* seedlings (Fig. 5D), suggesting that they also had reduced wall integrity.

Dye Effects on Plant Growth

To assess the physiological effects of S4B and 7GFE, seedlings were grown on agar plates containing the dyes. Plates containing 0.1% (w/v) S4B inhibited root growth, whereas on plates containing 0.01% S4B, seedling roots were consistently longer than wild type (Fig. 6, A and C). This increase in root growth might occur because the dye, which carries a negative charge, decreases cellulose crystallinity or its interactions with

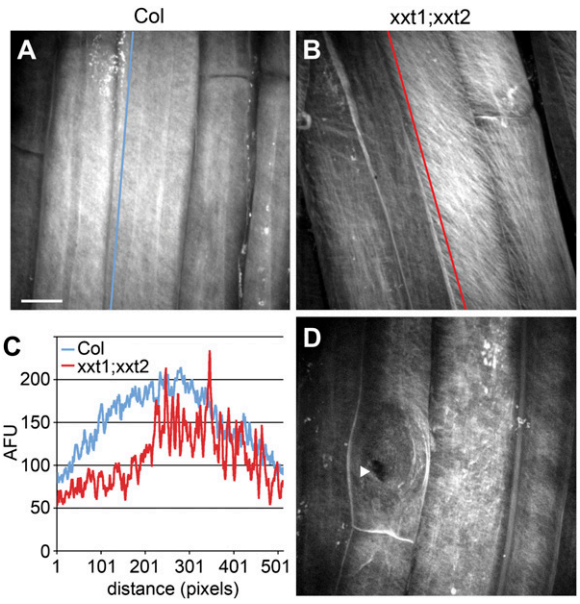

Figure 5. S4B staining pattern in *xxt1;xxt2* root cells. A, Col root elongation zone cells stained with S4B. B, *xxt1;xxt2* elongation zone cells showing striated fibrillar staining. C, Plot of fluorescence intensity along lines in A and B showing relatively even S4B staining profile in Col and uneven profile in *xxt1;xxt2*. AFU, Arbitrary fluorescence units. D, Differentiation zone cells showing rupture in trichoblast cell wall (arrowhead); note lack of bright staining at root hair primordium (bulged region around arrowhead). All images are maximum projections of z series. Scale bar in A applies to B and D and is 10 μm.

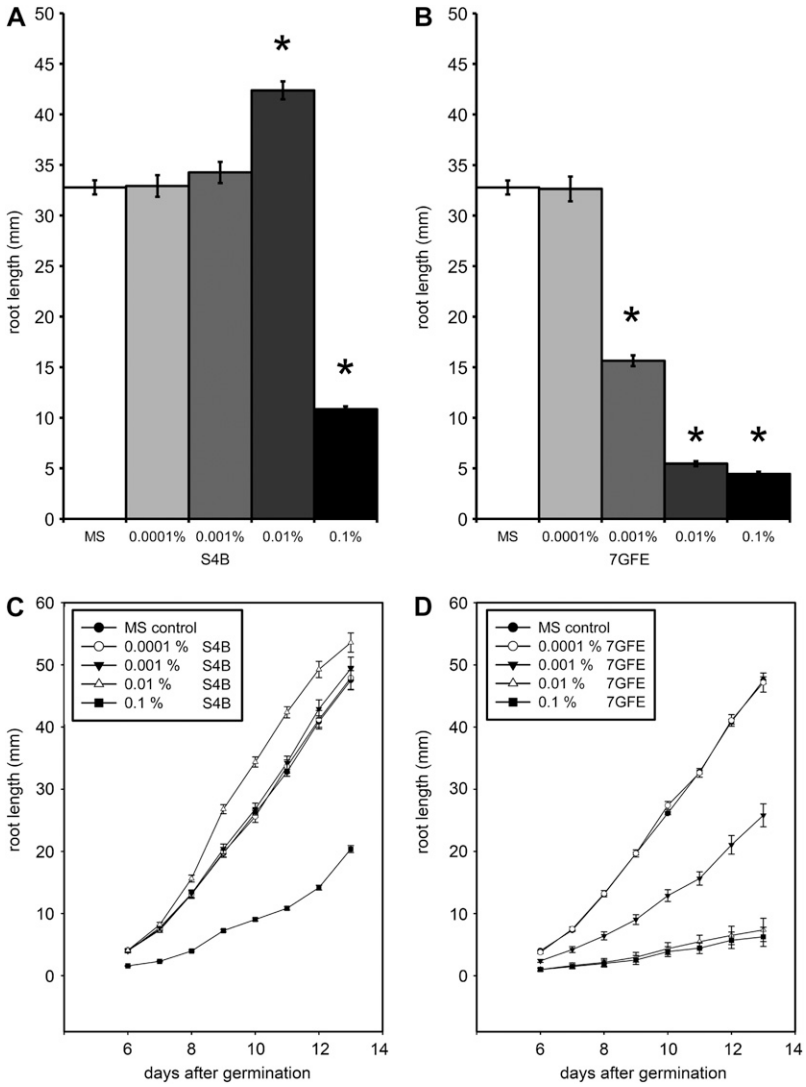

Figure 6. Effects of S4B and 7GFE on root growth. Seedlings were sown on plates with the indicated amounts (w/v) of S4B (A and C) or 7GFE (B and D). Primary root length was measured at day 11 in A and B. Asterisks indicate a significant difference from control ($P < 0.001$) in a two-tailed *t* test. MS, Murashige and Skoog medium.

hemicellulose, thereby allowing the cell wall to expand faster than normal. S4B had no significant effect on root growth at concentrations of 0.001% and 0.0001% (Fig. 6, A and C). 7GFE strongly inhibited root growth at concentrations higher than 0.0001%, practically abolishing root elongation at concentrations of 0.01% and higher (Fig. 6, B and D). In seedlings treated with 0.1% S4B, we observed that trichoblasts were significantly shorter (130 ± 35 μm versus 199 ± 60 μm, $P < 0.001$, two-tailed *t* test) and root hairs were significantly longer (696 ± 115 μm versus 429 ± 64 μm, $P < 0.001$, two-tailed *t* test) than in untreated controls. For the time-lapse experiments described above, an S4B concentration that did not inhibit root growth (0.01%) was used.

DISCUSSION

We have identified useful fluorescent dyes for labeling plant cell wall components. Because these dyes have low M_rs they should diffuse readily through the cell wall, which has an estimated porosity of about 3 nm (Chesson et al., 1997), unlike fluorescent proteins that are much larger and must withstand the acidic pH of the apoplast.

Spinning disc confocal microscopy of S4B-stained root cells allowed us to image cellulose orientation in three dimensions over time. Our results provide evidence that in some layers of the cell wall, cellulose microfibrils rotate in a transverse to longitudinal direction after their synthesis in anisotropically expanding root cells, as has been suggested for Arabidopsis hypocotyl cell walls (Refregier et al., 2004). The average strain rate of 30.8% for fiber rotation we calculated is in agreement with previous calculations of strain rate for whole Arabidopsis root cell walls (Beemster and Baskin, 1998), which suggests that passive reorientation of the fibers within the wall matrix in response to turgor pressure-driven cell expansion could be sufficient to explain the rotation we observed. This reorientation could play a role in wall relaxation in

response to the tension generated by sustained turgor pressure. It is also clear that wall modification, for example by expansin and XET activity, is critical for expansion (Cosgrove, 2005). The activity of these or other proteins could play a role in facilitating cellulose reorientation by selectively altering the degree to which cellulose microfibrils are cross-linked to one another and/or other wall components, thus altering the levels of strain required to cause cellulose reorientation. Our results differ from observations of cellulose architecture at the inner face of the cell wall after in vitro deformation that imply that the highly transverse cellulose microfibrils in that wall layer spread in a parallel fashion during wall extension (Marga et al., 2005). However, our results were collected from living cells and encompass all of the cell wall layers, and it is possible that coordinated parallel spreading and reorientation of cellulose microfibrils could occur in different wall layers under different conditions.

The ability to image cellulose architecture allowed us to structurally characterize the cell walls of mutants lacking either a cellulose synthase subunit or two xyloglucan xylosyltransferase isoforms. The gaps in S4B staining in *prc1-1* cells suggest that decreased cellulose content results in structural gaps in the cell walls of these mutants that are points of weakness in the wall. This result provides a potential explanation for why the cells of *prc1-1* seedlings are less able to channel intracellular turgor pressure into longitudinal growth. The increased spacing between S4B-stained fibers in the *xxt1;xxt2* mutant suggests that the interaction of xyloglucan with cellulose may be required to maintain the normal distribution of cellulose microfibrils in the cell wall. This observation provides support for the idea that hydrogen bonding of xyloglucan to cellulose microfibrils serves to prevent excessive hydrogen bonding of the microfibrils to each other, thereby facilitating cell wall expansion (McCann et al., 1990; Chanliaud et al., 2004).

The ruptures we observed in *prc1-1* and *xxt1;xxt2* trichoblasts suggest that these mutants have weak cell walls that can break under the strain caused by turgor pressure. One interpretation of these results is that S4B binding further weakens the walls of these cells, causing them to rupture. We are currently investigating whether this is the case and whether S4B might change the accessibility of cell wall components to degradation.

Based on the results described above and previous findings, we have generated a conceptual model of cellulose dynamics in the context of wall expansion (Fig. 7). The fibrillar S4B staining we observed in elongating root epidermal cells indicates that in these cells, cellulose is evenly distributed over the wall surface at large scales, but is unevenly distributed at the submicron scale. The fact that we could resolve this fibrillar structure using confocal microscopy, which has a resolution limit of a few hundred nanometers as compared to the tens of nanometers between cellulose microfibrils at the inner wall face as measured by scanning electron microscopy (Baskin et al., 1999; Sugimoto et al., 2000), suggests that at least some cellulose in the cell wall exists as bundles of closely spaced microfibrils with larger distances between them rather than the evenly spaced individual microfibrils depicted in most cell wall models (Somerville et al., 2004). In support of the former idea, 15 to 20 nm diameter bundles of cellulose have been observed at the outer surface of the cell wall by field emission scanning electron microscopy (Sugimoto et al., 2000), and cellulose macrofibrils have been observed by atomic force microscopy (Ding and Himmel, 2006). One potential source of small-scale anisotropy is the nature of cellulose synthesis: in expanding cells, multiple CESA particles move in opposite directions along single tracks (Paredez et al., 2006), presumably generating closely spaced parallel and antiparallel cellulose microfibrils. Cross-linking by secreted wall components such as hemicelluloses could be expected to occur predominantly between closely spaced cellulose microfibrils, whereas cross-linking between distant cellulose microfibrils might be less extensive. Our observation of thick fibrillar structures in lateral root cap and differentiating epidermal root cells suggests that cellulose microfibrils, after being synthesized in a relatively uniform sheet at the inner face of the cell wall (Baskin et al., 1999; Sugimoto et al., 2000), associate into larger bundles as cell wall expansion proceeds. The implication of this microfibril clustering (Paradez et al., 2006) is that microfibrils can reorient in bundles as the cell wall expands and new wall layers are synthesized beneath them (Fig. 7).

Because cellulose microfibrils are long rigid cables that are extremely strong under tension but are relatively weak against shear and compressive forces (Bruck et al., 2002), orienting cellulose microfibrils at a variety of angles would allow the cell to resist

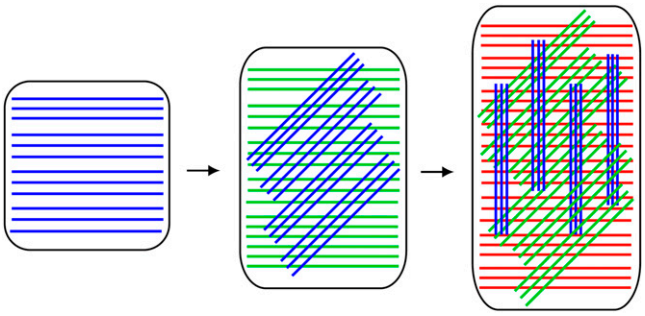

Figure 7. Model for cellulose microfibril dynamics during cell wall expansion. In a longitudinally expanding cell, newly synthesized cellulose microfibrils at the inner wall face (blue) contain small initial spatial inhomogeneities that are amplified as cell expansion occurs and the fibers rotate from transverse to longitudinal. The synthesis and rotation of subsequent cellulose microfibrils (green, red) beneath the initial cellulose microfibril layer result in a cell wall with cellulose microfibrils oriented at multiple angles. Note that cellulose microfibrils are not necessarily synthesized in discrete layers, and cellulose microfibril rotation does not necessarily occur immediately after synthesis.

internal and external forces from a variety of directions. Secondary cell walls achieve this by varying cellulose microfibril orientation in different wall layers. We propose that in primary cell walls, a multilayered network of cellulose microfibrils at different angles develops during cell expansion (Fig. 7). In our view, the reorientation of cellulose microfibrils, while it is a passive process that is driven by turgor pressure-induced wall elongation, is likely enabled by the activity of wall-loosening enzymes such as XETs and expansins (Cosgrove, 2005) that eliminate the physical constraints that would otherwise prevent reorientation from occurring.

Our results indicate that prior to elongation, cellulose microfibrils in the wall are oriented transversely relative to the long axis of the cell. This arrangement allows the cell wall to resist forces along its radial axis better than along its longitudinal axis. When combined with uniform turgor pressure, this results in anisotropic expansion. The importance of this architecture is demonstrated by the S4B staining pattern in *prc1-1* seedlings, where large gaps between fibers coincide with decreased anisotropic expansion. As the cell elongates, the reorientation of cellulose toward a longitudinal orientation might provide additional tensile strength in that dimension. This reorientation, in combination with the rigidification of other cell wall component networks, could eventually limit longitudinal expansion. In contrast, if longitudinally oriented cellulose microfibrils were synthesized at the membrane they could immediately constrain cell elongation. Generating a cell wall containing variously oriented cellulose microfibrils via transverse synthesis followed by expansion-driven microfibril rotation should be more efficient than synthesizing cellulose microfibrils in multiple orientations, then attempting to expand through them.

In summary, we have shown that cellulose microfibrils in the plant cell wall undergo a dynamic reorientation that results in the self assembly of a complex, multilaminate geometry in which differently angled layers arise from initially transverse microfibrils. This represents an elegant mechanism by which plant cells can allow anisotropic expansion to generate a structure capable of resisting force along any axis.

MATERIALS AND METHODS

Dye Characterization

7GFE was a gift from Huntsman International LLC. S4B (Hoch et al., 2005) was purchased from the Aldrich Rare Chemical Library (#S479896). Calcofluor and Congo red were purchased from Sigma. A set of carbohydrates consisting of extracted arabinan (sugar beet; Megazyme), arabinogalactan (larch; Megazyme), arabinoxylan (rye; Megazyme), curdlan (Sigma-Aldrich), galactomannan (guar; Megazyme), glucomannan (Konjac; Megazyme), isoprimeverose (Megazyme), lichenan (Icelandic moss; Megazyme), pectic galactan (lupin; Megazyme), mannan (borohydride reduced; Megazyme), rhamnogalacturonan (soybean pectic fiber; Megazyme), starch (potato; Sigma-Aldrich), xylan (larchwood; Sigma-Aldrich), xyloglucan (tamarind seed; Megazyme), and soluble cellobiose through cellohexose (Seikagaku) was used for the characterization. For 7GFE and S4B, enhanced fluorescence in the presence of carbohydrates was observed in solutions containing 50 to 150 mM NaCl or KCl. The solubility of Calcofluor and Congo red were significantly decreased in salt-containing solutions.

To determine which carbohydrates fluoresced when labeled with dye, 1 mg/mL solutions of the carbohydrates were dissolved or suspended in 0.01% solutions of the dye in PBS (7GFE, S4B), or water (Calcofluor) in 96-well plates. The fluorescence of each well was measured using the fluorescence cartridge of a paradigm detection system (Beckman Instruments) at excitations of 360, 485, 535, and 585 nm. Excitation at 485 and 535 nm was most informative for 7GFE and S4B, respectively, and excitation at 360 and 485 nm was informative for Calcofluor. Contour plots of dye fluorescence were recorded on a Jobin Yvon Horiba fluorimeter. Solutions of 0.001% S4B or 7GFE and 1 mg/mL cellulose or xyloglucan in 4 mL cuvettes were used. Excitation and emission were probed at 1 nm increments. The slot width for emitted light was 1 nm in each case. A slot width of 1 nm was used for excitation of 7GFE. The lower brightness of S4B necessitated a slot width of 10 nm for excitation of S4B. The signal from the fluorimeter was corrected for variations in mercury lamp intensity and a 1× PBS solution was used for blank subtraction.

Cell Wall Labeling

Arabidopsis (*Arabidopsis thaliana*) seeds of the Col ecotype, the *prc1-1* mutant (The Arabidopsis Information Resource germplasm no. CS297; Desnos et al., 1996), and the *xxt1;xxt2* mutant (The Arabidopsis Information Resource germplasm no. CS16349; Cavalier et al., 2008) were surface sterilized in 30% bleach in water with 0.1% SDS, washed four times in water, and suspended in 0.15% agar at 4°C in the dark for at least 2 d before planting. Seeds were germinated on vertical 0.8% agar plates containing 2.2 g/L Murashige and Skoog salts (Caisson Labs), 0.6 g/L MES, and 1% Suc (0.5× Murashige and Skoog medium) pH 5.6 in 24 h 120 μmol m^{-2} s^{-1} light at 21°C for 5 d. For cell wall labeling, seedlings were removed from the plate and placed in 1.5 mL microcentrifuge tubes containing 0.01% (w/v) S4B in liquid 0.5× Murashige and Skoog medium lacking agar for 30 min, washed one time with water, and mounted on slides for observation. Seedlings were observed using a 100× 1.4 NA oil immersion objective on a Leica SD6000 microscope attached to a Yokogawa CSU-X1 spinning disc head with a 561 nm laser and controlled by Metamorph software. Z series were recorded with a 200 nm step size and analyzed using ImageJ. Maximum projections of contiguous fields of view were stitched together using the MosaicJ plugin of ImageJ. Time-lapse recordings of stained cells with an interval of 1 min were made using 100 to 200 ms exposures and aligned using the stackreg plugin of ImageJ to correct for motion of the entire root.

Growth Measurements

Col seeds were sterilized as above and sown on 0.5× Murashige and Skoog plates containing 0.0001%, 0.001%, 0.01%, and 0.1% w/v 7GFE and S4B; root length was recorded from 6 to 13 d after germination.

Supplemental Data

The following materials are available in the online version of this article.

Supplemental Figure S1. 7GFE becomes highly fluorescent at different wavelengths with cellulose and xyloglucan.

Supplemental Figure S2. The fluorescence profiles of 7GFE with cellulose or xyloglucan.

Supplemental Movie S1. Time-lapse confocal microscopy reveals rotation of cellulose fibers in expanding Col root cells.

Supplemental Movie S2. Cellulose fiber rotation is not measurable in *prc1-1* root cells.

Supplemental Movies S3 and S4. Rupture of cell walls in *prc1-1* root cells.

ACKNOWLEDGMENTS

The authors thank Ken Keegstra for advice on the *xxt1;xxt2* mutant, Ian Wallace, Heidi Szemenyei, Clarisa Bejar, Ying Gu, and Tobias Baskin for

helpful comments on the manuscript, and members of the Somerville labs for helpful discussions.

Received October 27, 2009; accepted December 1, 2009; published December 4, 2009.

LITERATURE CITED

Baskin TI (2005) Anisotropic expansion of the plant cell wall. Annu Rev Cell Dev Biol **21:** 203–222

Baskin TI, Meekes HT, Liang BM, Sharp RE (1999) Regulation of growth anisotropy in well-watered and water-stressed maize roots. II. Role of cortical microtubules and cellulose microfibrils. Plant Physiol **119:** 681–692

Beemster GT, Baskin TI (1998) Analysis of cell division and elongation underlying the developmental acceleration of root growth in *Arabidopsis thaliana*. Plant Physiol **116:** 1515–1526

Boraston AB, Bolam DN, Gilbert HJ, Davies GJ (2004) Carbohydrate-binding modules: fine-tuning polysaccharide recognition. Biochem J **382:** 769–781

Bruck H, Evans J, Peterson M (2002) The role of mechanics in biological and biologically inspired materials. Exp Mech **42:** 361–371

Cavalier DM, Lerouxel O, Neumetzler L, Yamauchi K, Reinecke A, Freshour G, Zabotina OA, Hahn MG, Burgert I, Pauly M, et al (2008) Disrupting two *Arabidopsis thaliana* xylosyltransferase genes results in plants deficient in xyloglucan, a major primary cell wall component. Plant Cell **20:** 1519–1537

Chanliaud E, De Silva J, Strongitharm B, Jeronimidis G, Gidley MJ (2004) Mechanical effects of plant cell wall enzymes on cellulose/xyloglucan composites. Plant J **38:** 27–37

Chesson A, Gardner PT, Wood TJ (1997) Cell wall porosity and available surface area of wheat straw and wheat grain fractions. J Sci Food Agric **75:** 289–295

Cosgrove DJ (2005) Growth of the plant cell wall. Nat Rev Mol Cell Biol **6:** 850–861

Desnos T, Orbovic V, Bellini C, Kronenberger J, Caboche M, Traas J, Hofte H (1996) Procuste1 mutants identify two distinct genetic pathways controlling hypocotyl cell elongation, respectively in dark- and light-grown Arabidopsis seedlings. Development **122:** 683–693

Ding SY, Himmel ME (2006) The maize primary cell wall microfibril: a new model derived from direct visualization. J Agric Food Chem **54:** 597–606

Dolan L, Janmaat K, Willemsen V, Linstead P, Poethig S, Roberts K, Scheres B (1993) Cellular organisation of the Arabidopsis thaliana root. Development **119:** 71–84

Franks PJ (2003) Use of the pressure probe in studies of stomatal function. J Exp Bot **54:** 1495–1504

Green PB (1960) Multinet growth in the cell wall of Nitella. J Biophys Biochem Cytol **7:** 289–296

Hoch HC, Galvani CD, Szarowski DH, Turner JN (2005) Two new fluorescent dyes applicable for visualization of fungal cell walls. Mycologia **97:** 580–588

MacKinnon IM, Sturcova A, Sugimoto-Shirasu K, His I, McCann MC, Jarvis MC (2006) Cell-wall structure and anisotropy in procuste, a cellulose synthase mutant of Arabidopsis thaliana. Planta **224:** 438–448

Marga F, Grandbois M, Cosgrove DJ, Baskin TI (2005) Cell wall extension results in the coordinate separation of parallel microfibrils: evidence from scanning electron microscopy and atomic force microscopy. Plant J **43:** 181–190

McCann MC, Wells B, Roberts K (1990) Direct visualization of cross-links in the primary plant cell wall. J Cell Sci **96:** 323–334

Paradez A, Wright A, Ehrhardt DW (2006) Microtubule cortical array organization and plant cell morphogenesis. Curr Opin Plant Biol **9:** 571–578

Paredez AR, Somerville CR, Ehrhardt DW (2006) Visualization of cellulose synthase demonstrates functional association with microtubules. Science **312:** 1491–1495

Preston RD (1982) The case for multinet growth in growing walls of plant cells. Planta **155:** 356–363

Refregier G, Pelletier S, Jaillard D, Hofte H (2004) Interaction between wall deposition and cell elongation in dark-grown hypocotyl cells in Arabidopsis. Plant Physiol **135:** 959–968

Sauter M, Seagull RW, Kende H (1993) Internodal elongation and orientation of cellulose microfibrils and microtubules in deepwater rice. Planta **190:** 354–362

Singh SK, Fischer U, Singh M, Grebe M, Marchant A (2008) Insight into the early steps of root hair formation revealed by the procuste1 cellulose synthase mutant of Arabidopsis thaliana. BMC Plant Biol **8:** 57

Somerville C (2006) Cellulose synthesis in higher plants. Annu Rev Cell Dev Biol **22:** 53–78

Somerville C, Bauer S, Brininstool G, Facette M, Hamann T, Milne J, Osborne E, Paredez A, Persson S, Raab T, et al (2004) Toward a systems approach to understanding plant cell walls. Science **306:** 2206–2211

Stone B, Evans NA, Bonig I, Clarke AE (1984) The application of Sirofluor, a chemically defined fluorochrome from aniline blue for the histochemical detection of callose. Protoplasma **122:** 191–195

Sugimoto K, Williamson RE, Wasteneys GO (2000) New techniques enable comparative analysis of microtubule orientation, wall texture, and growth rate in intact roots of Arabidopsis. Plant Physiol **124:** 1493–1506

Taiz L (1984) Plant cell expansion: regulation of cell wall mechanical properties. Annu Rev Plant Physiol **35:** 585

Verbelen JP, Kerstens S (2000) Polarization confocal microscopy and congo red fluorescence: a simple and rapid method to determine the mean cellulose fibril orientation in plants. J Microsc **198:** 101–107

Vissenberg K, Fry SC, Pauly M, Hofte H, Verbelen JP (2005) XTH acts at the microfibril-matrix interface during cell elongation. J Exp Bot **56:** 673–683

Wood PJ (1980) Specificity in the interaction of direct dyes with polysaccharides. Carbohydr Res **85:** 271–287